Fusion Engineering and Design 159 (2020) 111770

Contents lists available at ScienceDirect

Fusion Engineering and Design

journal homepage: www.elsevier.com/locate/fusengdes

Recent progress in the design of the K-DEMO divertor

Sungjin Kwon[a,*], Kihak Im[a], Suk-Ho Hong[a], Hyungho Lee[a], Thomas D. Rognlien[b], William Meyer[b], Keeman Kim[a]

[a] National Fusion Research Institute, Daejeon 34133, Republic of Korea
[b] Lawrence Livermore National Laboratory, Livermore CA, 94551, USA

ARTICLE INFO

Keywords:
K-DEMO
Divertor
Edge plasma analysis
Electromagnetic analysis
Thermal analysis

ABSTRACT

The preliminary conceptual design of the Korean fusion demonstration reactor (K-DEMO) with a major radius of 6.8 m and the fusion power of 2200 MW has been studied since 2012. The overall configuration of the K-DEMO divetor system based on the ITER-like water-cooled tungsten technology is a double-null type symmetric divertor subdivided into 32 toroidal modules for the vertical maintenance. A detached divertor scenario with impurity seeding was considered as the primary approach for the power exhaust to reduce the peak heat flux lower than the engineering limit of 10 MW/m^2. The power exhaust performance at the scrap off layer was estimated by using UEDGE-2D code, a two-dimensional fluid transport code for collisional edge plasma and neutral species like N, Ne, and Ar. Particle and heat flux on inboard and outboard divertor targets were calculated for the detached cased depending on parameters such as the impurity seeding rate, pumping rate, and the pedestal density. On the other hand, a magnetic solution like X-divertor, snowflake divertor, and super X-divertor to expand the plasma wet area was considered for K-DEMO since the detached divertor increasing a radiation fraction by impurity seeding might be able to be unstable. However, the extremely high current of poloidal coils was required more than the engineering limit, 20 MA, to form magnetic field lines for the alternative divertors.

Based on the physical calculation of the edge plasma, engineering analyses were carried out to find out the thermal and structural reliability. The thermo-hydraulic analysis confirmed thermal stability, whether all comprising materials are operating within their allowable temperature windows when the case of the peak heat flux is set to 10 MW/m^2 on the outboard divertor target. The response surface optimization method derived two optimal design candidates employing two kinds of heat sink materials, respectively: the reduced activation ferritic martensitic (RAFM) steel and CuCrZr alloy. The drawbacks and merits of the two materials were definite. The optimal design with applying RAFM steel was vulnerable to withstand thermal and mechanical loads since low thermal conductivity caused too thin thickness of the heat sink. On the other hand, the CuCrZr alloy has critical drawbacks in terms of activation and radioactive waste despite its high thermal conductivity. Meanwhile, preliminary electromagnetic (EM) analysis was carried out to estimate the EM loads caused by the abnormal behaviors of plasma since EM loads are one of the most critical external loads for designing a DEMO divertor.

1. Introduction

A pre-conceptual design study for the Korean fusion demonstration tokamak reactor (K-DEMO) has been carried out since 2012 for 2200 MW of fusion power [1]. The heating power is 600 MW, comprising plasma heating from α-particle (~480 MW) and external auxiliary heating (~120 MW), as shown in Fig. 1. The major and minor radiuses of the plasma are 6.8 m and 2.1 m, respectively. The superconducting magnet system of K-DEMO consists of 16 toroidal field (TF) coils, 8 central solenoid (CS) coils, and 12 poloidal field (PF) coils. The magnetic field at the plasma center is about 7.4 T, and the peak field is as high as ~16 T. The plasma current is about 12 MA in steady-state operation. An up-down symmetric double-null configuration is applied as a primary choice for a study with high elongation of 2 and the triangularity of 0.625 [2].

The behavior of plasma and neutrals near the edge of the core plasma and adjacent to material surfaces plays a crucial role in the acceptability and performance of magnetic fusion devices. Power plant studies need to identify an acceptable tokamak design that can solve the high heat flux problem for plasma-facing components, including the divertor and the first wall. The plasma-wall interaction problem in the scrape-off layer (SOL) is also a critical issue for fusion. Thus, a key need

* Corresponding author.
E-mail address: sjkwon@nfri.re.kr (S. Kwon).

https://doi.org/10.1016/j.fusengdes.2020.111770
Received 20 September 2019; Received in revised form 13 May 2020; Accepted 15 May 2020
Available online 31 May 2020

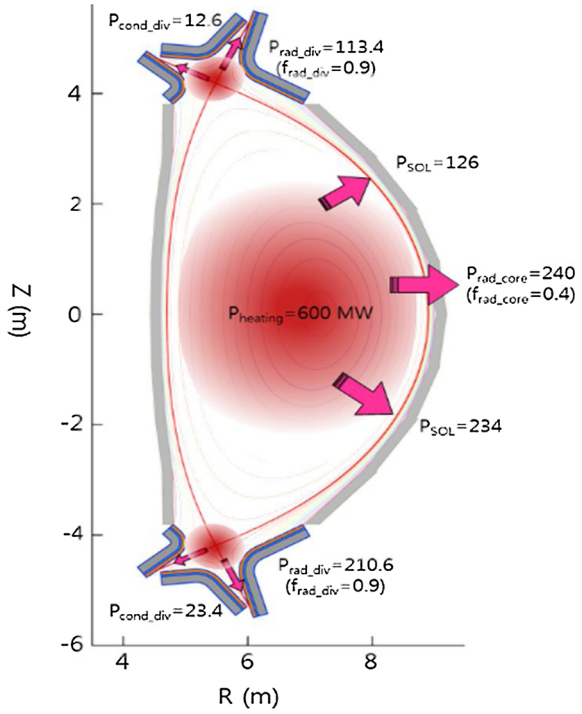

Fig. 1. Plasma power flow diagram for K-DEMO (unit in MW).

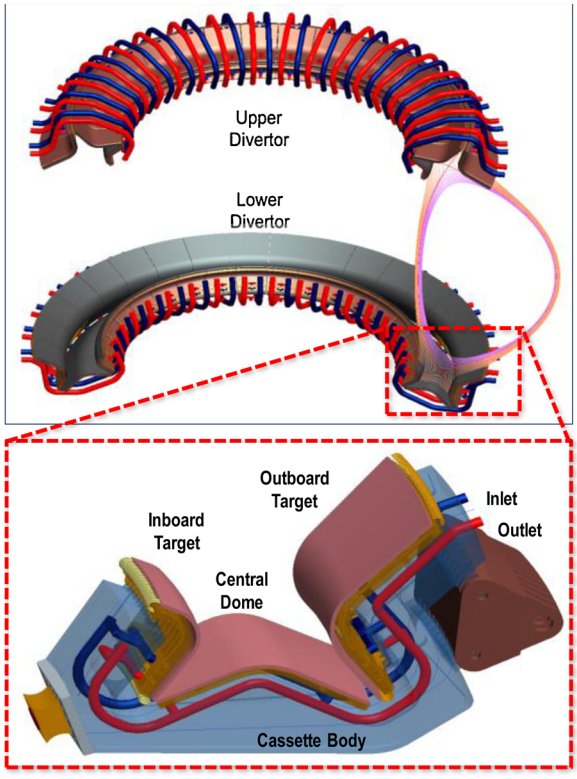

Fig. 2. K-DEMO divertor system (upper) and a divertor module structure (bottom).

of designs for future high-power devices is to identify and carefully analyze divertor strategies that can withstand or spread the exhaust heat flux to materials, thus making them available to be integrated into a self-consistent whole-device design.

In that sense, the divertor is one of the most critical and challenging in-vessel components in the fusion reactor. The purpose of the DEMO divertor is different from the divertor of other experimental devices, including ITER, although the current concepts of DEMO divertor are similar to ITER. The thermal power on divertor should be converted to electricity for electric efficiency since the purpose of DEMO is to prove the feasibility as a next-generation power plant. DEMO divertor is used in a limited operation scenario because it is used in a continuous operation environment, so the duty cycle should satisfy a ~ 70% level. Also, the lifetime of the DEMO divertor is important because periodic maintenance is required. The lifetime of the current divertor is estimated to be about two fpy [3]. Besides, divertor in maintenance should be discharged as low-level radioactive waste. Therefore, the materials comprising the DEMO divertor must meet these requirements, unlike other experimental devices. Moreover, DEMO devices would be operated in a high neutron dose environment. Although different for each material, ~ 10 dpa/fpy levels are expected, so structural damage under high neutron irradiation should be considered in the selection of materials [4].

The K-DEMO divertor system has the upper and lower divertors in symmetry (see Fig. 2). Upper and lower divertors are subdivided into 32 toroidal modules, respectively, to align with the blanket toroidal segmentation for the vertical maintenance [2]. Each 11.25° module of the upper or lower divertor consists of an inboard target, a central dome, and an outboard target. The targets are tilted with the poloidal angle between the targets and flux surfaces to 10° and 11.5°, for the outboard and inboard targets, respectively, to accommodate the conceived engineering limit of ~10 MW/m^2 of peak heat flux. The inlet/outlet cooling manifolds for each module deliver the pressurized water coolant to the outboard target, the central dome, and the inboard target in parallel manners.

Overall configurations of other DEMO divertor concepts are similar to the ITER divertor system employing the water-cooled tungsten monoblock concept. EU DEMO and CFETR apply CuCrZr alloy for the heat sink like ITER [5,6]. Therefore, the power on the divertor is not applicable to generate electricity since the coolant pressure and temperature are lower than the conditions of the pressurized water reactor (PWR). The detailed explanation will be mention in Section 3.1. On the other hand, the Japanese DEMO divertor system has a unique feature employing two types of heat sink materials [7]. CuCrZr alloy is applied at the target around the peak heat flux region to enhance the cooling capability, and RAFM steel is used at baffle and dome are with PWR condition coolant. The concept efficiently utilizes both the cooling and electricity generation. However, joining the gap between the two regions looks challenging at the engineering point.

2. Divertor SOL simulation using UEDGE

For the divertor SOL analysis in K-DEMO, the UEDGE-2D code was employed [8,9]. UEDGE implements a multi-species fluid model, solving the plasma density, the ion and electron velocities, and the ion and electron temperatures in the full toroidal geometry of 2D magnetic equilibria. The most important empirical input to UEDGE is the anomalous radial transport coefficients, which can be represented by spatially varying diffusion and convection coefficients. To account for kinetic effects, a flux-limited form of the classical parallel transport coefficients calibrated by kinetic calculations is used. The output from UEDGE includes plasma heat and particle fluxes to all surrounding surfaces, including the divertor and main-chamber walls. Varying shapes of divertor surfaces are accommodated directly via a body-fitting mesh capability, and single-null and double-null divertor configurations can be simulated. Both transient and steady-state simulations can be performed. The neutral gas model generally used in UEDGE is flux-limited fluid neutral atomic and, for hydrogen, molecular species that includes charge-exchange and elastic scattering, among other neutrals and ions. This neutral model is periodically calibrated with more detail Monte Carlo neutral simulations by DEGAS 2 [10]. Impurity

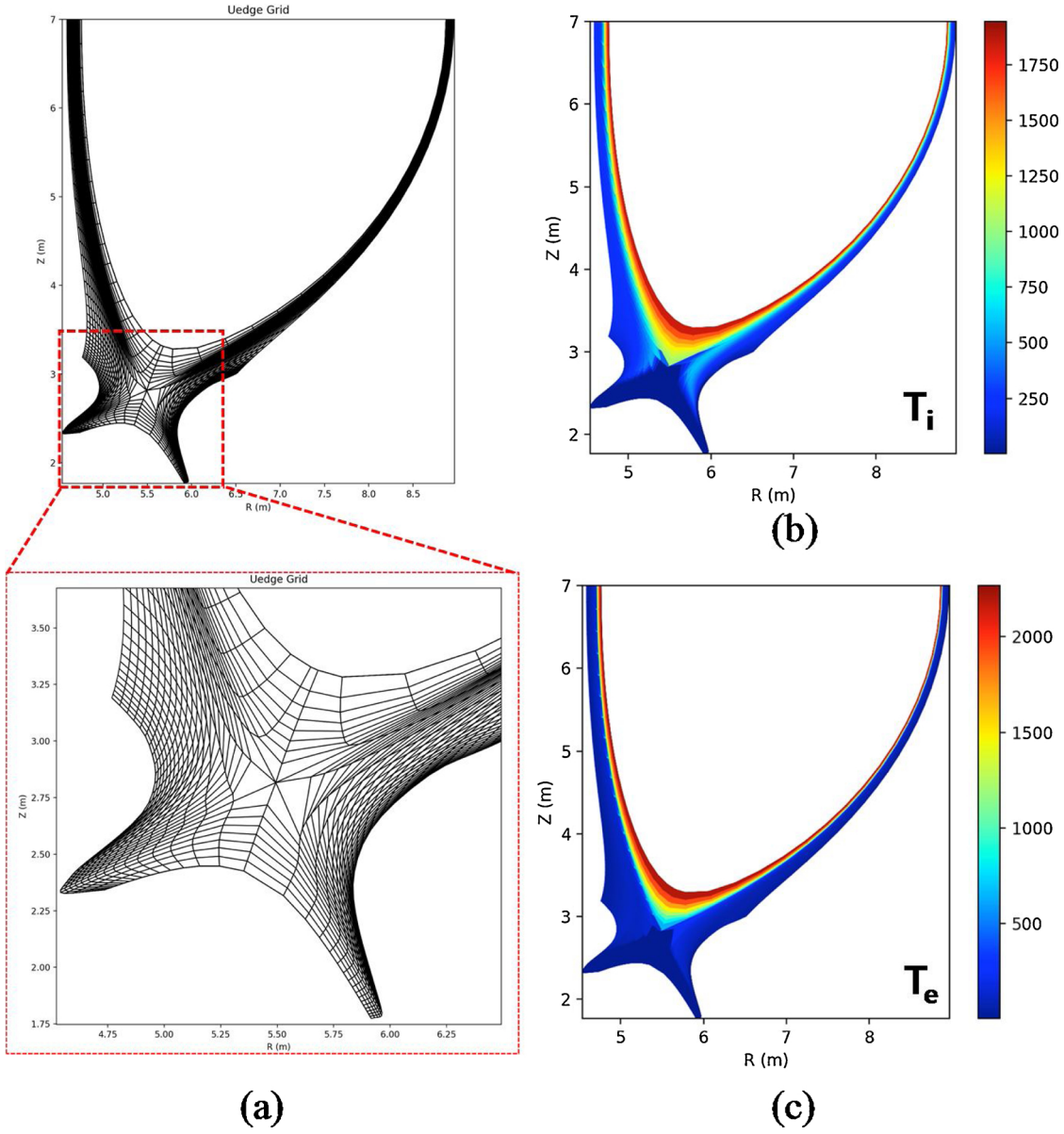

Fig. 3. (a) Non-orthogonal mesh for UEDGE calculation of K-DEMO divertor (b) ion temperature distribution and (c) electron temperature distribution for heating power, 600 MW with neon 1.4%.

ions and neutrals are also included, giving power loss from line radiation as well as fuel (deuterium/tritium) fuel dilution.

Here the input plasma core power into the lower-half edge region of the assumed symmetric up/down double null is 300 MW each in the electron and ion channels. The plasma density on the core-edge boundary is set to 1×10^{20} m^{-3}. The anomalous radial diffusion coefficients representing turbulence-induced fluxes are the following: 0.333 m^2/s for particles, 1.0 m^2/s for parallel ion velocity, and 0.5 m^2/s for ion and electron energy; these transport coefficients are kept constant in all of the simulations. The simulations are performed with an assumed concentration of impurities (Ne, N, Ar) relative to the DT ion density. The corresponding radiative energy loss in the electron channel is calculated from a coronal equilibrium model, including charge-exchange with the DT gas [11]. The DT gas is weakly pumped on the private-flux wall at the rate of $n_g v_{tb}(1\text{-}albedo)$, $v_{tb} = [T_g/(2\pi m_g)]^{1/2}$ is the one-sided thermal gas flux. The electron and ion temperatures are shown in Fig. 3 (b) and (c) for Ne 1.4% with *albedo* = 0.99945.

First, the maximum heat flux was calculated in the divertor target as the plasma heating power is changed. Fig. 4 (a) shows the maximum heat flux at inner and outer targets when the density of Ne impurity is 0.4%, and *albedo* is 0.99. As the heating power increases, the heat flux increases. At 600 MW of K-DEMO's heating power, the peak heat flux of the outer target is about 33 MW/m^2, which is much larger than 10 MW/m^2, which is generally known as engineering limit. Therefore, it is necessary to reduce the heat flux by making the detached divertor by adjusting the type and density of the impurity and *albedo*. Fig. 4 (b) and (c) show the tendency of maximum heat flux according to the density of Ar and Ne impurity, respectively. It can be seen that the peak heat flux decreases as the radiation heating increases with the increase of the neutral particles. Fig. 4 (d) shows the trend of heat flux with *albedo*. The increase in *albedo* lowers the pumping of the neutral particles, thus increasing radiation and making the detached divertor lowering the heat flux.

From this sensitivity study, it has been shown that the boundary plasma density at the mid-plane hardly changes during the scan of the impurity concentration. However, the plasma densities at the divertor targets decrease when the impurity concentration increases. Interestingly, the electron temperature at the inner target shows no

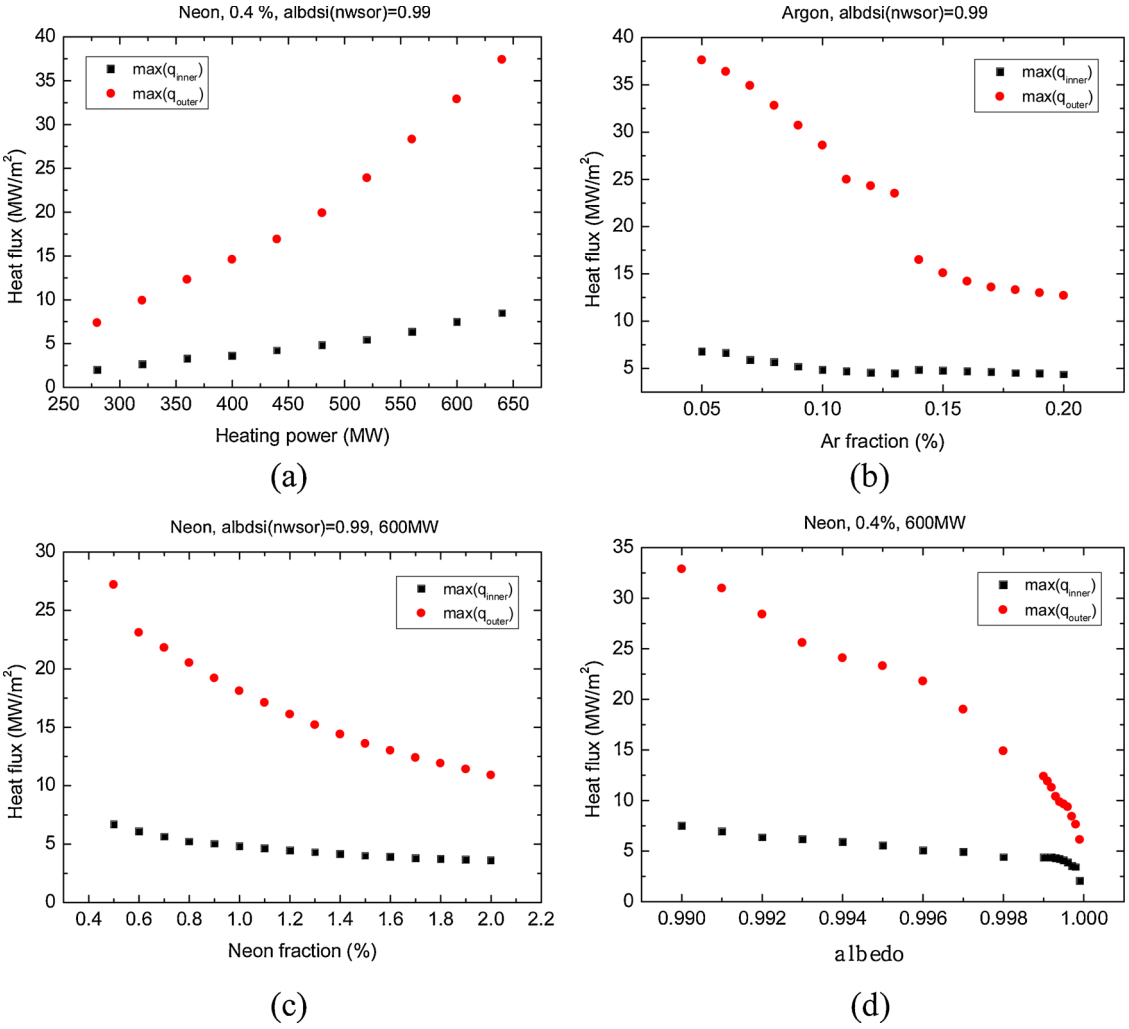

Fig. 4. Parameter studies for peak heat flux with respect to (a) heating power, (b) argon density fraction, (c) neon density fraction, (d) albedo.

significant change when the impurity concentration increases while the electron temperature at the outer target decreases significantly. For example, for the Ne concentration scan, the electron temperature at the outer target changes from 3.14 eV to 1.56 eV when the concentration changes from 0.4% to 2.0%. It is also found that the neutral density at the outer target increases substantially from 4.45×10^{19} m^{-3} to 2.16×10^{20} m^{-3}. It implies that the higher neutral density with higher Ne concentration leads to the significant loss of the plasma energy until it reaches the outer target, resulting in the significant reduction of the outer target peak heat flux, as shown in Fig. 4(c). These behaviors of the plasma parameters are similarly recognized during the scan of albedo. When albedo increases (the pumping rate decreases), since the remaining neutral density can be larger at the outer target region, the target peak heat flux is significantly reduced with albedo, as shown in Fig. 4(d).

During the heating power scan, the boundary plasma density at the mid-plane does not change. However, the boundary plasma electron temperature increases with the heating power, as expected. The plasma densities at both divertor targets slightly increase with the heating power, while only the electron temperature at the outer target increases significantly with the heating power. It is noted that the neutral density at the outer target region decreases with the heating power, while the neural density at the inner target region increases. It is suspected that this significant difference in the neural densities causes a faster increase in the peak heat flux at the outer target, as shown in Fig. 4(a).

Next, when the heating power was 600 MW, and N, Ne, and Ar impurity were applied, the heat flux profile according to the inner and outer target position was calculated. In each case, the change of heat flux and the location of peak heat flux were observed by changing the density and *albedo* of the impurity. Fig. 5 is the analysis result according to each impurity type. First, as the density of impurity increases, the peak heat flux generally decreases. However, increasing the *albedo* rather than the density of the impurity is a more important parameter for lowering the peak heat flux. Overall, the maximum heat flux was significantly reduced in the case of *albedo* 0.99945 rather than 0.99. Also, the position where the peak heat flux occurs is moved behind the target, creating a detached divertor. Although it is not practical to create an environment in which *albedo* grows extremely large, we are studying to lower the peak heat flux by implementing detached divertors in various ways.

Although it still needs further investigation on which impurity species is better for the divertor detachment scenario, the present UEDGE simulation study has shown that higher-Z impurities can be more efficient in achieving the detachment regime. Especially, it has been found that a full detachment at the outer target can be obtained with less concentration of Ar compared to N and Ne, as shown in Fig. 5. But, in the present simulation, the concentration is just an input parameter. Whether a certain level of Ar concentration can be maintained experimentally is still uncertain. Furthermore, it has been known that higher-Z impurity penetrates into the core plasma and leads to the radiative collapse of the plasma more easily. Then, the proposed scenarios by the simulation study should be tested experimentally, and reliable

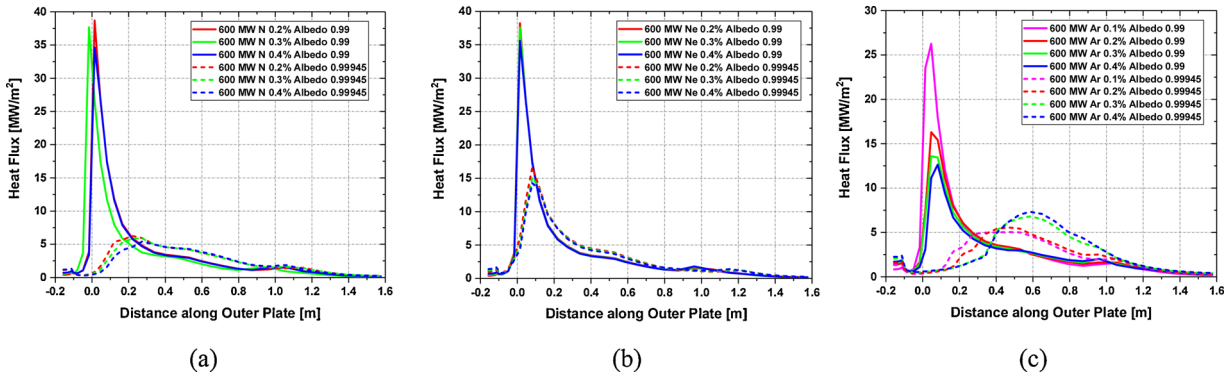

Fig. 5. Heat flux profiles for albedo and density fraction and types of impurities: (a) nitrogen, (b) neon, and (c) argon.

operation scenarios have to be developed. This still remains as future work.

3. Engineering approach

3.1. Heat sink material for the DEMO divertor

The coolant tube used as the heat sink should effectively transfer the heat loads to the coolant. Thus, high thermal conductivity is the most important material property for a good heat sink material. High yield/ultimate strength and elastic modulus at high temperature and corrosion resistance are also required since the heat sink has to play a role as a structural material. In that sense, CuCrZr is the most attractive material for the heat sink since it has a high thermal conductivity of 357 W/m·°C at room temperature [12]. However, there are waste concerns regarding the use of copper materials in the fusion neutron environment. The results of the report calculated by CCFE are cited for activation analysis according to Cu usage [13]. Copper in the K-DEMO divertor region is predicted to have a medium level of radioactivity after hundreds of years after shutdown when irradiated with neutrons for 2 fpy (full power year). (See Fig. 6) Moreover, the operating temperature window of CuCrZr is relatively narrow, 200 ~300 °C [12]. Due to the narrow operating temperature range, the coolant of PWR (the condition cannot be applied, so that it is not proper to generate electricity. Therefore, RAFM steel has been considered as another candidate for the heat sink in the DEMO to make up for the weak points of CuCrZr.

RAFM steel has been selected because it is a low activated material.

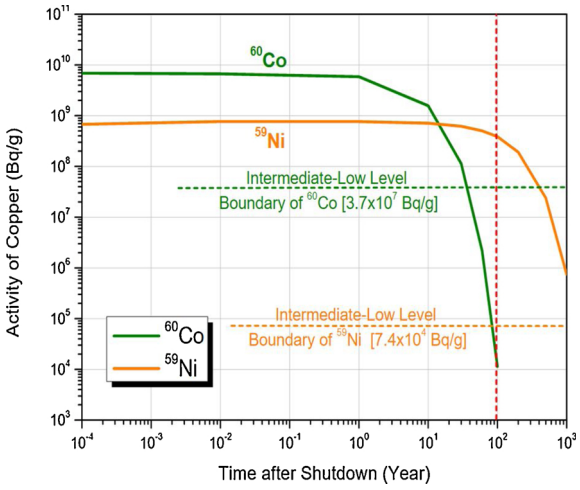

Fig. 6. Activity by 60Co and 59Ni nuclides transitioned from 1 g of copper irradiated to neutrons for 2 fpy in the K-DEMO divertor region (NWL = ~ 1.82 MW/m^2).

Furthermore, the PWR condition can be applied to RAFM steel because it has a wide and high operating temperature window of 300-550 °C [14]. In addition, the mechanical properties of RAFM steel, such as elastic modulus, yield strength, and the ultimate strength, are better than those of CuCrZr. However, RAFM steel is not a useful material in terms of heat transfer because of its poor thermal conductivity of 26 W/m °C at room temperature. In K-DEMO divertor, RAFM and CuCrZr have been considered as the first and second candidates of heat sink material, respectively.

3.2. Nuclear analysis of structural damage

Neutrons from the plasma cause the material damages expressed through displacement per atom per full power year of operation (dpa/fpy). Generally, displacement damage is strongly dependent on the threshold displacement energy of materials, and neutron fluxes in specific tally volumes [15]. The MCNP code was used on the displacement damage calculation using the simple and accurate analysis methods, and nuclear heating calculations with FENDL-2.1 nuclear data library [16]. The ADVANTG code for Monte Carlo simulations to generate variance reduction parameters was used in this calculation to reduce computing time and effort due to the iterative calculations [17].

In Fig. 7 (a), the maximum damage is indicated by a value of 10.9 dpa/fpy on the RAFM heat sink material above the OT top [4]. Although RAFM was further away from the plasma, the displacement damage at RAFM (10.9 dpa/fpy) was higher than tungsten (2.6 dpa/fpy). This is due to the lower critical energy of RAFM than tungsten (RAFM ~ 40 eV, W ~90 eV). Copper material as a heat sink in the lower OT area was performed because this area has a relatively lower rate of displacement damage by RAFM material than others. The heat sink in the lower OT area was subdivided into eight tally volumes to compare detailed displacement damage using RAFM and copper materials (see Fig.7 (b)). In Fig. 7 (c), the displacement damage of the RAFM and the copper material gradually increased upward. In addition, copper materials exhibit ~ 56% higher displacement damage rates than RAFM materials. However, because copper materials are less exposed to neutrons in the plasma, the rate of displacement damage is much lower than in other parts (see Fig. 7 (a)).

3.3. Thermomechanical analysis

Thermomechanical analysis with the aid of statistical estimation is carried out to find out the thermally and mechanically reliable structure of the K-DEMO divertor target. Firstly, the design parameter correlation was accomplished to define the relations between input and output parameters. Based on the correlation, DoE (design of experiment) was done to derive the response surfaces. The response surfaces provide the expected values of the output parameters, everywhere in the range of selected input parameters without performing CFD (computational fluid dynamics) analyses. Based on the response surfaces, the optimum

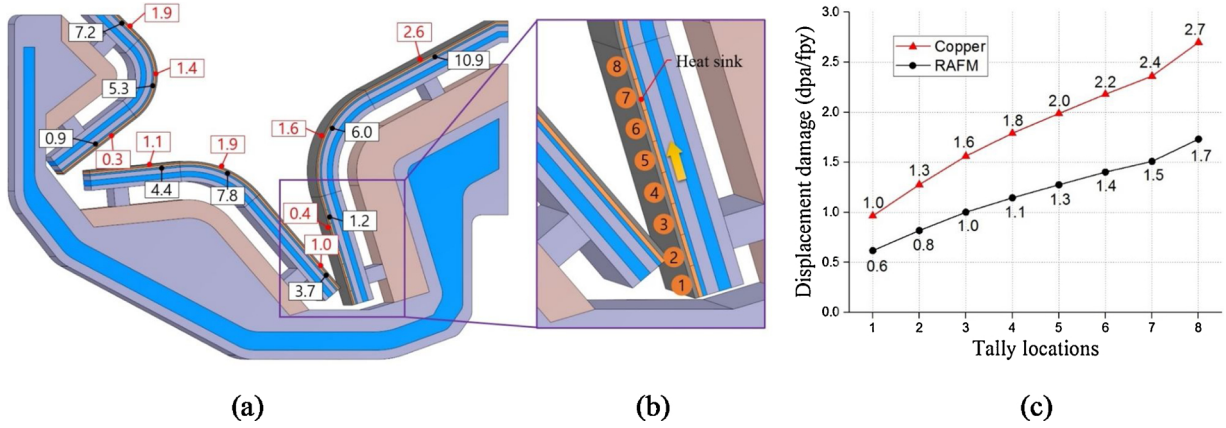

Fig. 7. (a) The maximum displacement damage on tungsten armors (red) and RAFM heat sinks (black) of K-DEMO divertor system, (b) a detail view of lower OT area, (c) Comparison of calculated displacement damage rates between copper and RAFM materials in the heat sink of lower OT (For interpretation of the references to color in this figure legend, the reader is referred to the web version of this article).

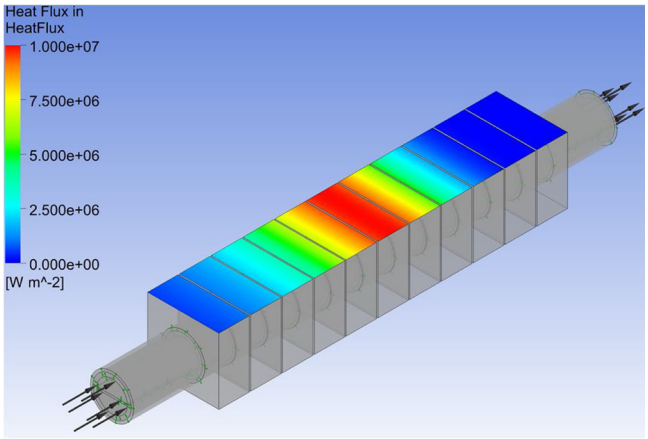

Fig. 8. Heat flux distribution of peak heat flux10 MW/m2 for CFD analysis.

designs were derived from two models employing RAFM steel and CuCrZr. Heat flux on the divertor target and the simulation model is shown in Fig. 8.

The objectives and constraints of the input and output parameters were applied to derive the optimum design by using the response surfaces. The maximum allowable temperature of tungsten that is a key constraint in the optimization study was set to 1250 °C to avoid recrystallization [18,19]. Every constraint and objective of the CuCrZr and RAFM models are the same except for the constraint condition of the maximum temperature of the heat sink, CuCrZr < 300 °C [12], and RAFM < 550 °C [14]. The inlet conditions, including temperature and pressure of the coolant, are 290 °C, 15 MPa for the RAFM model, and 70 °C, 4 MPa for the CuCrZr model. The coolant speed is set 15 m/s for two models to operate below the critical heat flux [18]. For both models, candidates satisfying the objectives and constraints were suggested by the ANSYS/DesignXproler, as shown in Table 1. Fig. 9 shows the results of CFD analyses for the selected candidate of each model. The results showed that both models didn't exceed the material's maximum allowable temperature ranges. However, the T_{tube} of the RAFM model was 0.25 mm, too thin [18].

Thermomechanical analyses were performed with ANSYS to verify the structural stability of the optimized models with the derived parameters and dimensions meeting the thermal requirement. Three kinds of the model are set up to observe the structural stability; 11 monoblocks with 3 supports, 11 monoblocks with 4 supports, and 11 monoblocks with 6 supports. (See Fig. 10) Temperature distribution calculated from CFD analysis is employed by using a one-way fluid

Table 1
The suggested optimum design parameters and the results for the CuCrZr and RAFM models.

Design Parameters		The Candidate of Parameter Optimization	
		CuCrZr Model	RAFM Model
Input Parameters	T_{top}	8.7 mm	5.1 mm
	T_{lat}	6.5 mm	3.2 mm
	T_{tube}	1.0 mm	0.25 mm
	Coolant condition at inlet	4 MPa, 70 °C	15 MPa, 290 °C
Output Parameters	Max. temperature of monoblocks	1241.9 °C	1172.8 °C
	Max. temperature of heat sink	270.6 °C	550.0 °C

structural interaction (FSI) method. Coolant pressures of 15 MPa for the RAFM model and 4 MPa for the CuCrZr model are also applied at the inside of the cooling tube. Finally, the pseudo- electromagnetic force is applied on the plasma-facing surface of tungsten monoblock from 1 kN to 10 kN as a distributed tension force.

Fig. 11 shows the maximum stress of heat sink obtained by thermomechanical analyses for two models; the RAFM model and CuCrZr model. In the case of the RAFM model, the tube thickness was very thin (0.25 mm) to meet the thermal requirements, exceeding the allowable stress in the EM force in all sections. On the other hand, the CuCrZr model showed maximum stress lower than the allowable stress in all EM force sections. Therefore, it is not suitable to use RAFM as a heat sink to cool 10 MW/m2 in terms of structural robustness.

3.4. Electromagnetic analysis

The current quench and the thermal quench occur during plasma disruption or vertical displacement events caused by the abrupt instability of plasma or the failure of control occurs. Due to the sudden change of the plasma current, the induced currents of eddy current and halo current are generated at the in-vessel components such as vacuum vessel, blanket, and divertor. EM force caused by the induced currents is one of the most important external load which has to be considered in the design.

Fig. 12 shows the sector model of K-DEMO with a periodicity of 22.5° along the toroidal direction for EM analysis. The divertor cassette body attaches to the vacuum vessel with inner and outer supports. The numbers of elements and nodes are 978,916 and 1,861,991, respectively. The sector model can save computing resources without

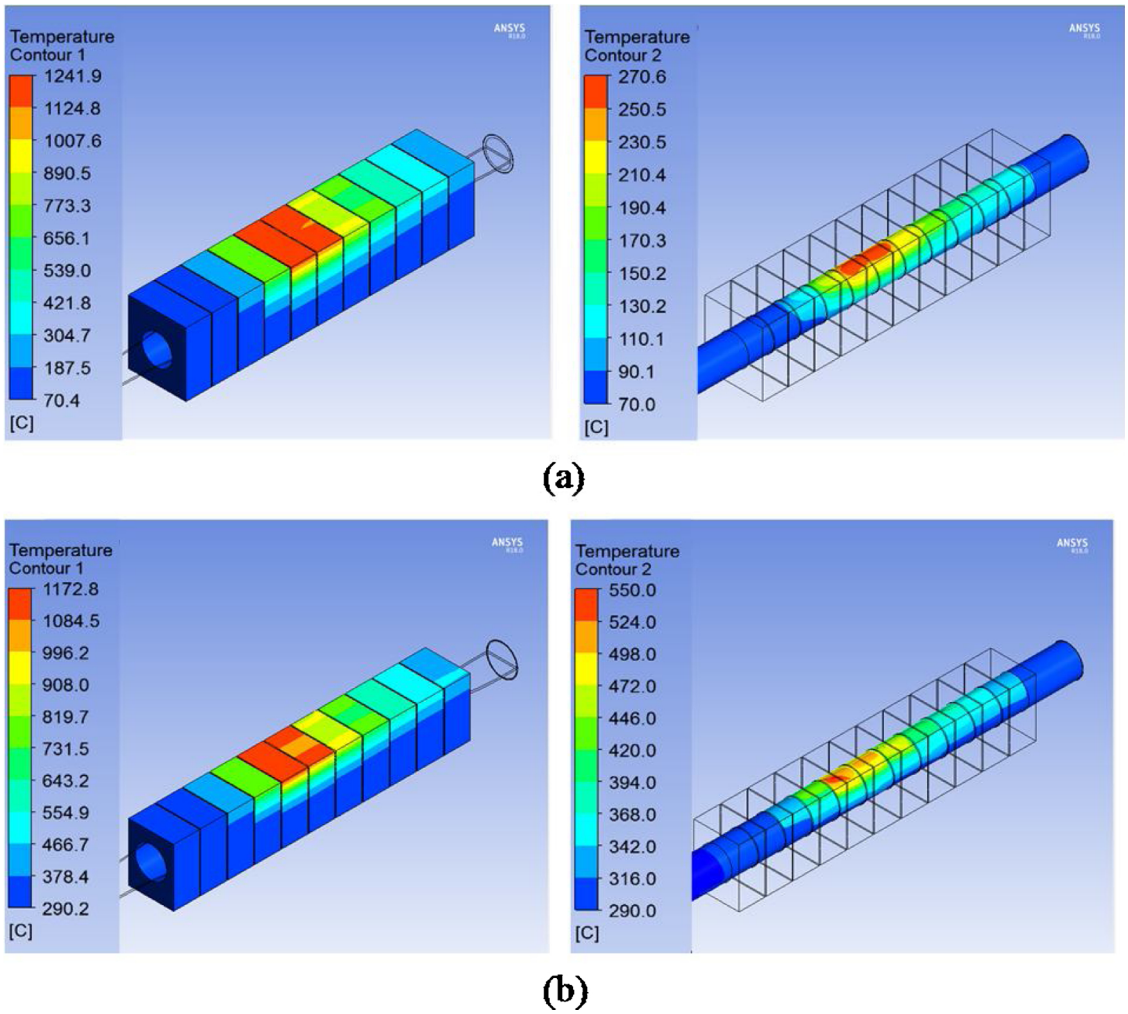

Fig. 9. Temperature distribution of monoblocks and heat sinks in CFD validation results for (a) the CuCrZr model, (b) the RAFM model.

sacrificing physical phenomena by applying periodic boundary conditions for magnetic vector potential and electric potential on the cutting face of the sector model [20,21]. The magnetic flux parallel condition along the central axis is also included.

The EM loads carried by a downward major disruption (MD) exponential 16 ms event have been evaluated. Since the scenario for the MD event of KDEMO has not been developed yet, the variation of the plasma current was converted from the ITER-based scenario (MD DW exponential 16 ms) by using the in-house code. The plasma currents of ITER and K-DEMO are 15 MA and 12 MA, respectively. The MD plasma current profile for time is derived by the ratio of plasma current between ITER and K-DEMO, as shown in Fig. 13 (a) [22]. Next, the most important input of EM analysis is geometrical plasma current at a specified time step. DINA calculation provides the input data for ITER. The first wall of ITER and K-DEMO are divided into fine grids to convert the data to K-DEMO. Finally, the geometrical plasma current data of K-DEMO is obtained by the 1:1 mapping of every grid. Fig. 13 (b) indicates the plasma current distribution at a specific time during the event.

Fig. 14 (a) and (b) shows the distributions of magnetic flux density and eddy current, respectively. Fig. 14 (c) and (d) shows the EM loads and moments vs. time acting on the divertor module during the MD event. The peak values of Fx, Fy, and Fz at the center of the divertor module are about 650 kN, −551 kN, and −306 kN, respectively. The

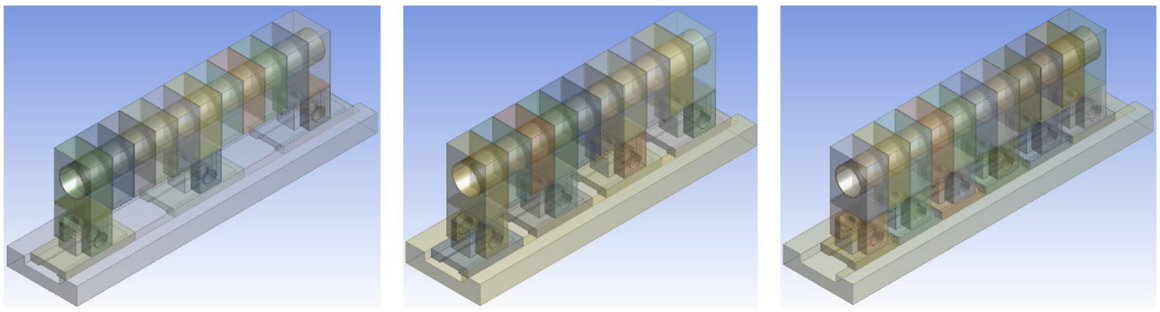

Fig. 10. Models for thermomechanical analysis; (a) 11 monoblocks with 3 support, (b) 11 monoblocks with 4 support, (a) 11 monoblocks with 6 support.

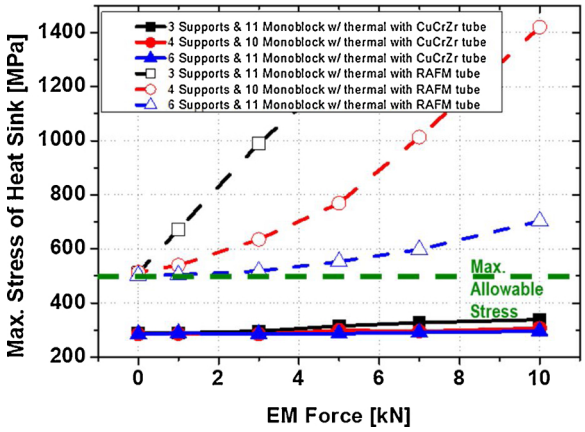

Fig. 11. Maximum stress of heat sink for there thermomechanical models under pseudo EM loads for CuCrZr (solid) and RAFM (dash).

level of peak values is similar to ITER, although materials and plasma current and configuration are different from ITER [20]. The further engineering analyses are on-going, and the EM loads induced by the halo current will be included. The stress analysis and structural stability assessment caused by the EM loads also will be carried out based on the EM analyses.

4. Alternative divertor concepts for K-DEMO

As progress in magnetic fusion yields better core confinement, the standard divertor (SD) is forced to operate more closely to full detachment to mitigate the resultant heat flux intensity at the target. A higher radiation fraction in the divertor region will likely be required in DEMO devices to deposit the exhaust heat over a larger area. Full detachment, however, has been experimentally observed to be unstable; the detachment front tends to migrate upstream from the target back to the core plasma, leading to MARFEs. Therefore, a magnetic solution to the "divertor bottleneck" may become a more attractive option, embodied by the X-divertor (XD) [23], snowflake divertor (SFD) [24], super X-divertor (SXD) [25]. Alternative divertor concepts would reverse these effects magnetically by creating a flux tube that flares as it approaches the target plate.

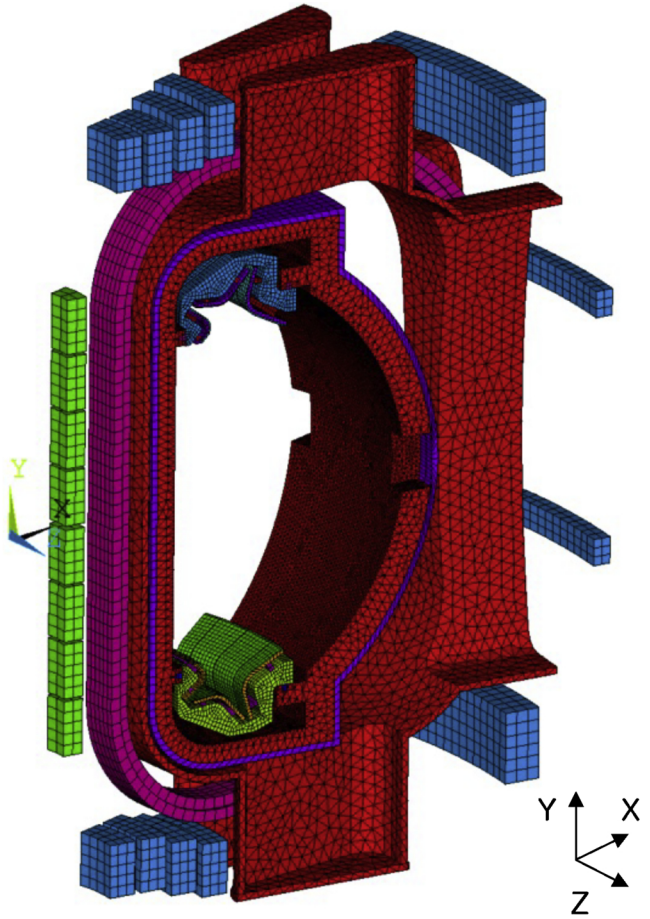

Fig. 12. The 22.5° sector FE model of K-DEMO for the EM analysis.

The application of in-vessel coils using Cu is not considered due to the rad-waste problem in the K-DEMO. The CS coil and the PF coil, as shown in Fig. 15 (a), are arranged to apply a vertical maintenance concept. The feasibility of SXD and SFD is considered for the K-DEMO magnet system. Fig. 15 (b) shows the magnetic field line of SOL in case of SD of double null type, and Fig. 15 (c) and (d) are SXD and SFD, respectively. The coil currents are summarized in Table 2 for SD, SXD, and SFD. As mentioned earlier, the currents on coils 1–10 and 11–20 are the same because of the K-DEMO up-down symmetry configuration, respectively. In general, it is impossible to apply a current of higher than 20 MA per coil due to the limitation of the manufacturing length of the superconducting magnet. SD meets the constraint, but SXD and SFD do not. Therefore, the application of SXD and SFD in K-DEMO is difficult without resolving the constraint, the limitation of the superconducting magnet.

5. Summary

The conceptual study on the K-DEMO has been started since 2012 for 2200 MW of fusion power. The preliminary concepts of main tokamak components have been developed, and the results for the divertor system were presented herein. A vertical maintenance scheme is chosen for the in-vessel components. With the pressurized water as a primary choice for the tokamak coolant, the key aspects of the divertor system have been studied.

The change of heat flux, according to the type and density of impurity and *albedo*, was observed using the UEDGE code. The detached divertor was studied by increasing radiation with changing impurity density and pumping rate. Therefore, the peak heat flux was reduced, and the position where the peak occurred moved backward. N, Ne, and Ar impurities were tested when the heating power was 600 MW, and Ar was the most promising impurity to reduce the peak heat flux.

Next, neutronics analysis and thermomechanical and electromagnetic analysis were performed from the perspective of K-DEMO engineering. The importance and pros and cons of RAFM steel and CuCrZr, major candidates of heat sink materials in DEMO divertors, have been proven. A dpa analysis was performed on both materials, and structural damages were evaluated in a neutron irradiation environment. Cu showed ~56% higher dpa than RAFM steel. Models for thermomechanical analysis using RAFM steel and CuCrZr were created, and CFD analysis was carried out around the peak heat flux zone. The response surface optimization method was applied to find a design that ensures thermal stability. The thermally optimized design was obtained for both models by this method, and thermomechanical analysis was performed by one-way FSI. The result showed the tube thickness of the RAFM model was very thin, 0.25 mm due to its low thermal conductivity, and the maximum stress exceeded the allowable stress. On the contrary, the CuCrZr model with proper tube thickness was structurally stable thanks to the high thermal conductivity of CuCrZr. However, the application of Cu alloy in DEMO devices has some issues such as radioactive waste and electric generation efficiency, so the choice between CuCrZr and RAFM is still open for the K-DEMO divertor. Next, the preliminary electromagnetic load calculation of the K-DEMO divertor has been carried out for the downward MD scenario by using ANSYS mechanical/Emag solver. The 22.5° sector model of K-

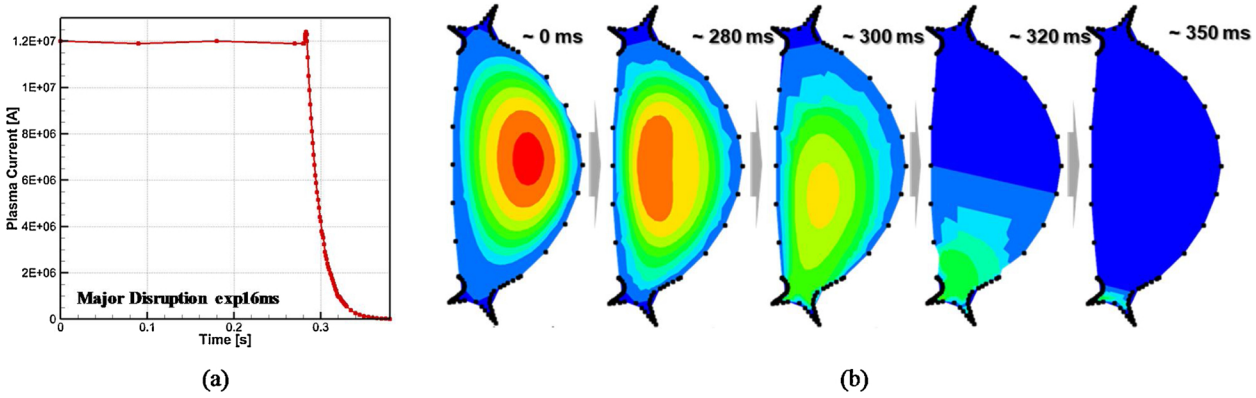

Fig. 13. (a) The variation of plasma current of MD DW exponential 16 ms for K-DEMO, (b) The plasma current distributions of K-DEMO during the major disruption at specific time.

DEMO was developed, and the magnetic flux parallel condition along the central axis and the periodic boundary conditions were applied. The in-house code to convert the variation of the plasma current during the MD event from the ITER scenario was developed. As a result, the maximum EM load of 650 kN occurred along the radial direction.

Finally, we reviewed the applicability of alternative divertor concepts, one of the ways to lower the peak heat flux in DEMO devices. XD, SXD, and SFD reduce the heat flux by expanding the peak heat flux region concentrated through the magnetic solution. K-DEMO reviewed the application of SXD and SFD under the precondition that vertical maintenance and in-vessel coil were not applied basically. However, implementing SXD and SFD required applying a high current of 20 MA to the coil considered to be difficult at present because of the manufacturing limitations of superconducting magnets.

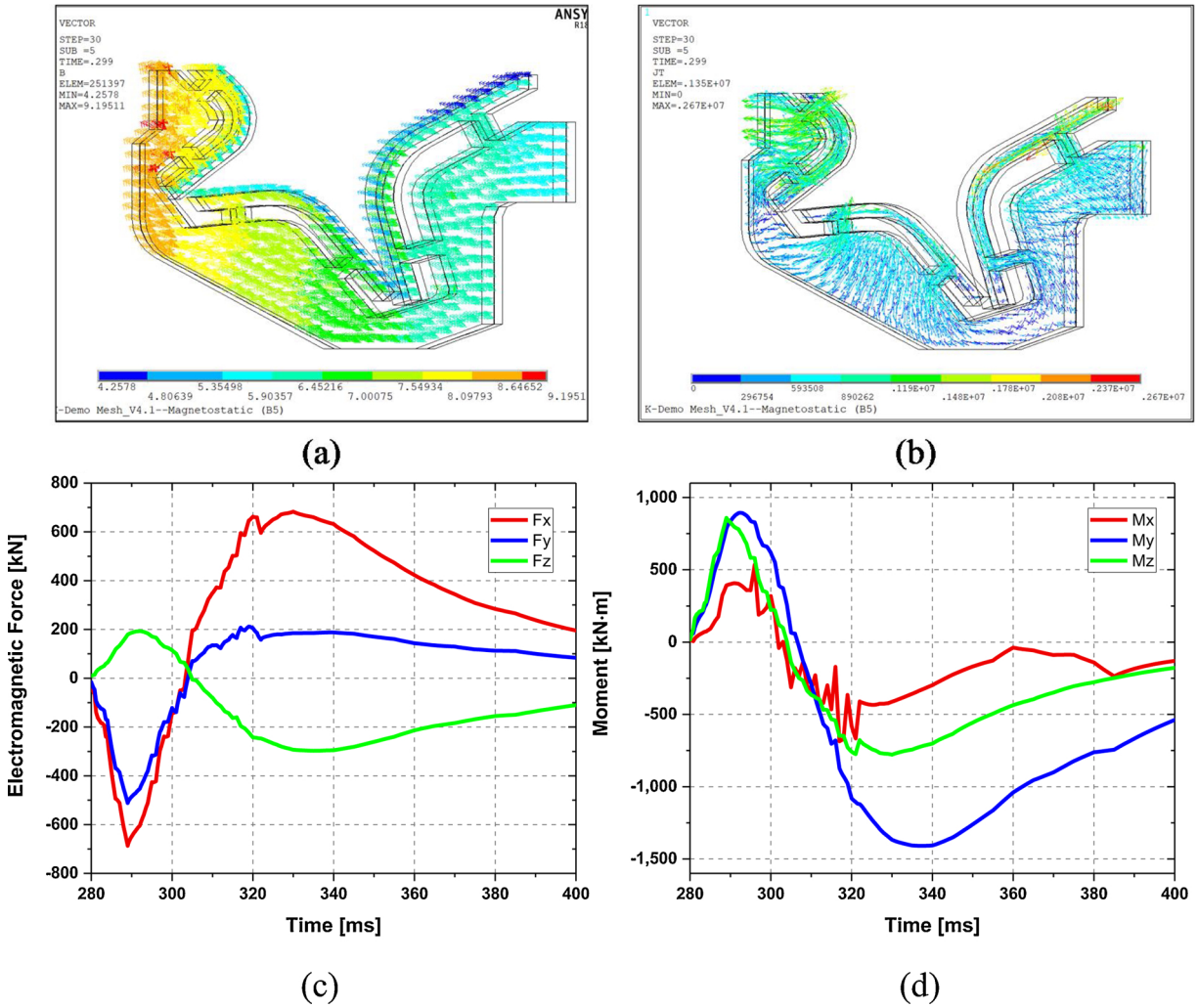

Fig. 14. Distributions of magnetic flux density (a) and eddy current (b) on the divertor. The (a) EM forces and (b) moments at the center of the divertor module during the MD event.

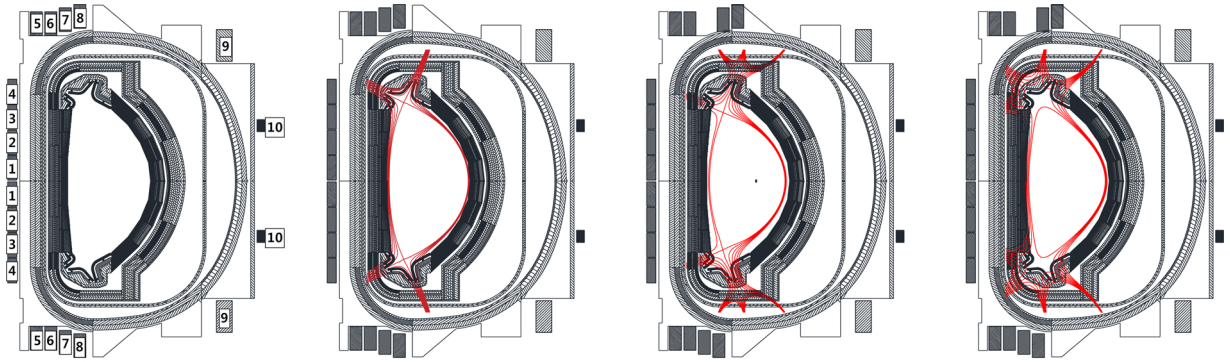

Fig. 15. (a) K-DEMO superconducting magnet system. Equilibrium magnetic field lines for (b) K-DEMO SD, (c) SXD, (d) SFD.

Table 2
Coil position and current for SD, SXD, and SFD.

Coil No.	R [m]	Z [m]	SD [MA]	SXD [MA]	SFD [MA]
1	1.638	0.7	11.4	16.3	4.6
2	1.638	2.1	5.9	9.6	25.2
3	1.638	3.5	2.3	20.8	−0.6
4	1.638	4.9	3.4	10.0	−26.2
5	2.98	8.31	−3.5	−46.5	−5.6
6	3.66	8.31	−4.6	12.7	25.2
7	4.34	8.59	−4.5	105.2	21.6
8	5.02	8.75	−4.1	−107.1	−57.5
9	12.96	7.5	8.4	31.2	36.1
10	14.88	2.95	2.6	−3.5	−8.6

Declaration of Competing Interest

None.

Acknowledgments

This work was supported by R&D Program through National Fusion Research Institute (NFRI) funded by the Ministry of Science and ICT, the Republic of Korea, (CN1901)

References

[1] K. Kim, K. Im, H.C. Kim, S. Oh, Y.S. Lee, J.S. Park, S. Kwon, et al., Design of K-DEMO for near-term implementation, Nucl. Eng. 55 (2015) 053027.
[2] K. Im, S. Kwon, J.S. Park, A preliminary development of the K-DEMO divertor concept, IEEE Trans. Plasma Sci. IEEE Nucl. Plasma Sci. Soc. 44 (2016) 2493–2500.
[3] D. Maisonnier, et al., DEMO and fusion power plant conceptual studies in Europe, Fusion Eng. Des. 81 (2006) 1123–1130.
[4] J. Park, K. Im, S. Kwon, J. Kim, D. Kim, M. Woo, C. Shin, Nuclear analysis of structural damage and nuclear heating on enhanced K-DEMO divertor model, Nucl. Eng. 57 (2017) 126044.
[5] J.H. You, G. Mazzone, E. Visca, et al., Conceptual design studies for the European DEMO divertor: rationale and first results, Fusion Eng. Des. 109–111 (2016) 1598–1603.
[6] X. Peng, M. Ye, Y. Song, et al., Engineering conceptual design of CFETR divertor, Fusion Eng. Des. 98–99 (2015) 1380–1383.
[7] K. Tobita, N. Asakura, R. Hiwatari, et al., Design Strategy and Recent Design Activity on Japan's DEMO, Fusion Sci. Technol. 72 (2017) 537–545.
[8] T.D. Rognlien, J.L. Milovich, M.E. Rensink, G.D. Porter, A fully implicit, time dependent 2-D fluid code for modeling tokamak edge plasmas, J. Nucl. Mater. 196–198 (1992) 347.
[9] T.D. Rognlien, M.E. Rensink, Edge-plasma models and characteristics for magnetic fusion energy devices, Fusion Eng. Des. 60 (2002) 497.
[10] T.D. Rognlien, M.E. Rensink, D.P. Stotler, Scrape-off layer plasma and neutral characteristics and their interactions with walls for FNSF, Fusion Eng. Des. 135 (Part B) (2018) 380–393.
[11] D.E. Post, A review of recent developments in atomic processes for divertors and edge plasmas, J. Nucl. Mater. 220–222 (1995) 143.
[12] J.-H. You, A review on two previous divertor target concepts for DEMO: mutual impact between structural design requirements and materials performance, Nucl. Eng. 55 (2015) 113026–113037.
[13] Mark R. Gilbert, Jean-Christophe Sublet, Robin A. Forrest, Handbook of activation, transmutation, and radiation damage properties of the elements simulated using FISPACT-II & TENDL-2014; Magnetic Fusion Plants, CCFER 15 (2015) 26.
[14] Antonella Li-Puma, Marianne Richou, Philippe Magaud, Marc Missirlian, Eliseo Visca, Vincenzo Pericoli Ridolfini, Potential and limits of water cooled divertor concepts based on monoblock design as possible candidates for a DEMO reactor, Fusion Eng. Des. 88 (2013) 1836–1843.
[15] R.L. Greenwood, R.K. Smither, SPECTER: Neutron Damage Calculations for Materials Irradiations Argonne National Laboratory Report ANL/FPP/TM-197, (1985).
[16] The IAEA Nuclear Data Section 2004 FENDL-2.1 Fusion Evaluated Nuclear Data Library, INDC (NDS)-467, Vienna, Austria, (2020).
[17] S.W. Mosher, et al., ADVANTG - an Automated Variance Reduction Parameter Generator Oak Ridge National Laboratory ORNL/TM-2013/416 Rev.1, (2015) http://info.ornl.gov/sites/publications/files/Pub46035.pdf).
[18] S. Kwon, K. Im, J. Park, Thermo-hydraulic optimization study for a high heat flux unit of the K-DEMO divertor target, Fusion Eng. Des. 134 (2018) 68–73.
[19] G.D. Rieck, Tungsten and its Compounds, first ed., Pergamon Press, 1967, p. 62.
[20] S. Park, H. Jhang, D.-K. Oh, D.Y. Ku, Electromagnetic load calculation of the ITER machine using a single finite element model including narrow slits of the in-vessel components, Fusion Eng. Des. 88 (2013) 3224–3237.
[21] Y. Lee, D.Y. Ku, D.W. Lee, M.-Y. Ahn, Y.-H. Park, S. Cho, Electromagnetic analysis of the Korean helium cooled ceramic reflector test blanket module set, Fusion Eng. Des. 109–111 (2016) 389–397.
[22] S. Kwon, K. Im, Y. Lee, S.-H. Hong, Preliminary electromagnetic loads calculation for the divertor of K-DEMO, Fusion Eng. Des. 146 (2016) 2135–2139.
[23] M. Kotschenreuther, P.M. Valanju, S.M. Mahajan, J.C. Wiley, On heat loading, novel divertors, and fusion reactors, Phys. Plasmas 14 (2007) 072502.
[24] D.D. Ryutov, V.A. Soukhanovskii, The snowflake divertor, Phys. Plasmas 22 (2015) 110901.
[25] P.M. Valanju, M. Kotschenreuther, S.M. Mahajan, J. Canik, Super-X divertors and high power density fusion devices, Phys. Plasmas 16 (2009) 056110.